KSME

Springer

Journal of Mechanical Science and Technology 37 (2) 2023

Original Article
DOI 10.1007/s12206-023-0129-y

Keywords:
· Desalination
· Hydration layer
· Molecular dynamics simulation
· Nanopore
· Steric effect

Correspondence to:
BoHung Kim
bohungk@ulsan.ac.kr

Citation:
Mahmud, M., Kim, B. (2023). Atomic boundary position and steric effects on ion transport and separation through nanoporous graphene membrane. Journal of Mechanical Science and Technology 37 (2) (2023) 875~886.
http://doi.org/10.1007/s12206-023-0129-y

Received March 18th, 2022
Revised October 4th, 2022
Accepted October 17th, 2022

† Recommended by Editor Chang-Soo Han

Atomic boundary position and steric effects on ion transport and separation through nanoporous graphene membrane

Morshed Mahmud and BoHung Kim

School of Mechanical Engineering, University of Ulsan, Daehak-ro 93, Nam-gu, Ulsan 680-749, Korea

Abstract The electrostatic attraction between ions and water is the primary reason for the change in ion bare diameter, which plays a crucial role in saltwater transportation. This study utilizes molecular dynamics (MD) to analyze saltwater transport through a nanoporous graphene membrane by pressure-driven flow. In this work, we describe the impact of pore diameter atomic boundary position on single-ion transportation and signify the steric effect of ions on the water mass flow rate and velocity profile. Due to hydration layer formation, ions hinder the water molecules from their regular velocity, which also decreases the flow rate of water molecules. Interestingly, a significant deviation for different atomic boundary positions is observed for ion rejection for pore diameters less than 1 nm. However, for larger pore diameters, the ion rejection closely matches the atomic boundary position specified by a 2 % water density drop inside the nanopore.

1. Introduction

Since only 3 % of the world's water is freshwater, it is becoming difficult to meet the water demands of the expanding population of the world [1, 2]. However, ocean water can meet this demand if it is desalinated. In this regard, it is necessary to assess the significance of saltwater desalination as a permanent water supply option [3].

Despite the fact that the reverse osmosis (RO) system is the most common desalination process due to low energy consumption, it needs to be advanced in terms of cost and efficiency [4-6]. Advances in nanotechnology opened up a new door for water desalination. When nanopore diameters are less than the size of the hydrated diameter of the ion (the entire boundary of the hydrated ion along with the hydration sphere around it), that ion can be excluded from the transportation by a size-exclusion mechanism [7]. Ion dehydration barriers, along with this size-exclusion mechanism, can lead to effective water desalination [8-10].

Choosing a membrane material for the nanopore is a delicate task because the membrane material needs to withstand the pressure created by the flow. Also, the membrane surface must be impermeable except for the nanopore area. Among all the candidate materials, graphene has these unique characteristics. Graphene blocks all kinds of molecules as it is composed of sp^2 hybridized carbon atoms in a 2D honeycomb lattice with a high electron density in its aromatic rings. The high carbon-carbon bond energy and intrinsic mechanical strength make graphene a supreme impermeable membrane [11]. Since the lattice constant of graphene is smaller than the molecular diameter of water, graphene is impermeable to ionic aqueous solution [12]. The sp^2 hybridized carbon atoms are structured like a hexagonal lattice structure; this single-atom thickness (0.34 nm) material is considered a critical material due to its remarkable mechanical strength and robustness [13, 14]. Due to this fact, specifically engineered graphene sheets have become the most promising new material for polymer electrolyte membrane fuel cells (PEMFC) applications [15]. Besides this, graphene-based fuel cell catalysts are also very efficient for both anode and cathode fabrication [16].

Given the above facts, creating a nanopore on a graphene membrane can effectively retain

the increased size of hydrated ions due to the steric effect, while the water molecules can pass through the nanopore successfully. Graphene membranes are still durable in pressure-driven flow after crafting the pore. In fact, a nanoporous graphene (NPG) membrane can withstand pressures exceeding 57 MPa, when having a nanopore smaller than 1 μm [17]. These nanopores can be functionalized, and the nanoporous membrane can be used in multi-layers. However, the water permeability depends on the pore spacing in this case [18].

The low energy consumption effect of nanoporous graphene membranes allows the flow of the desired molecules while blocking the contaminated particles. Hence, seawater ions can be effectively rejected using these single layer or multi-layer NPG membranes while purifying a significant amount of water [4]. NPG membranes have already been utilized as effective filters for desalination in a lot of recent molecular dynamics studies focusing on saltwater transport driven by pressure. However, the desalination efficiency of the NPG membrane is highly dependent on selective pore size, selective pressure, and pore hydrophobicity [19].

There is disagreement about how to select the pore diameter for desalination in recent studies. For example, Cohen-Tanugi et al. mentioned that a maximum pore diameter of 5.5 *Å* was necessary to prevent salt ion transport in their MD model of the reverse osmosis water desalination process using a NPG membrane, while Konatham et al. reported that a maximum pore diameter of 7.5 *Å* was needed to retard the salt ions [20, 21]. Later on, Nguyen et al. achieved 100 % salt rejection with a 9.90 *Å* pore diameter using a 35.02 MPa pressure drop [12]. This ongoing discussion on selecting the nanopore diameter remains since the definition of the nanopore diameter (visually the pore width) is still a debatable issue. The pore radius is defined in diverse ways on the nanoscale for different reasons [22]. The deep impact of the hydrated ion boundary can greatly influence on determining the pore diameter for effective water desalination. In fact, the hydration layer beyond the first hydration layer is also responsible for retaining the ion transport through the nanopore.

The internal energy barrier for ion transport depends on the pore radius, which can be affected by the proper boundary position of the nanopore. The effective pore radius was also defined by the width that forces the hydration layer to be partially broken for ion transportation [23, 24]. By investigating the hydration properties, it is possible to evaluate the hydrated solute steric hindrance and so predict an approximate pore size that may work adequately for effective water filtration [25]. Thus, it is necessary to have a deep understanding of the pore boundary position in relation to the hydration layers to predict saltwater transportation.

Ion mobility in the pore is smaller than the bulk ion mobility because they have a layered liquid structure in the pore axial direction [26]. When an ion hits the pore and wants to leave the bulk, it requires sufficient energy to overcome the energetic penalty. The energetic penalty progressions are subjected to the ion hydration, ion charge, pore chemical characteristics, pore size, and pore geometry [27-29]. Deformation of the reactive zone can happen when the sterically demanding group is close to the reactive center [30]. Ions show a gel-like property in an aqueous form, and the shape of this gel can change under pressure. Moreover, the strength of the ion's hydration depends on the ionic concentration and other environmental factors like ionic strength, pH, and temperature [31]. Due to these factors, the ion is partially dehydrated when the ion hydration strength becomes weak. These partially or fully dehydrated ions are transported through the nanopore. This dehydration is the primary source of the ion energy barrier for transportation in narrow pores [32].

The water molecules around small cations remain practically fixed in terms of distance, forming a shell where bulk water molecules continuously replace individual water molecules in nanoseconds [33, 34]. Because of the electric field of the ion, the solvent dipoles in the first hydration layer are highly structured, and the diploes around it do not act linearly [35, 36]. For this reason, the first layer of the hydration layer can be intact when transporting a cation through a pore radius of 1.2 nm, whereas the second layer can be partially dehydrated due to the pore wall [24]. When the ion is at the pore center, the hydration sphere around the ion will be dehydrated depending on the pore radius [37]. Therefore, it is necessary to assess the energy barrier for dehydration in relation to the atomic boundary position of pore diameter more extensively for predicting ion transportation.

In this paper, we mainly sought to investigate how the atomic boundary position of pore diameter impacts water and ion transportation prediction using molecular dynamics (MD) study. The steric effect of ions on water transportation was also studied. The primary objective of understanding the influence of the atomic boundary position of pore diameter on chlorine ion transportation has been analyzed by comparing a theoretical ion rejection proposed method with MD predicted ion rejection.

2. Theoretical background and model description

2.1 Molecular dynamics simulation

In Fig. 1(a), the simulation domain has saltwater on the left side (feed side) and pure water on the right side (permeate side). The volumes of both regions are kept static using a specular reflection wall, as represented in Fig. 1(c). In the beginning, two specular reflection boundaries were made rigid at Z = -4.4925 nm and Z = 4.4925 nm, while the x and y directions in the simulation domain were periodic with lengths of 3.192 nm and 2.952 nm. The graphene membrane was placed at the center at 0.0 nm in the z-direction, and a circular pore of 0.99 nm diameter was generated by removing the carbon atoms, as shown in Fig. 1(b).

Initially, this pore diameter L was considered from the atomic center to the center of carbon atoms inside the pore. The typical wall works like a piston to induce pressure-driven flow and

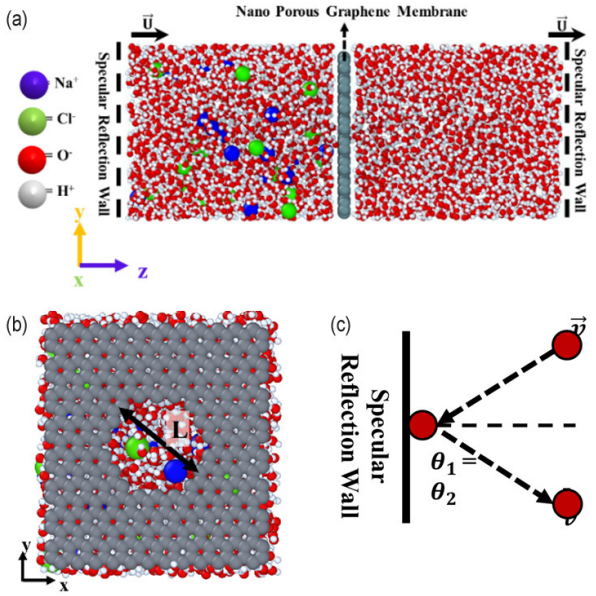

Fig. 1. (a) Schematics of the simulation domain; (b) the initially considered diameter L of graphene nanopores; (c) physical description of the specular reflection wall.

may interrupt the bulk pressure in the feed and permeate regions in the atomic level framework because of the van der Waals interactions between the fluid and piston [38-40]. Nonetheless, the specular reflection walls used with computationally compelling strategies can settle the issue [12, 40]. Thus, to avoid imprecise pressure drop across the simulation domain, a specular reflection wall is chosen instead of using a piston. The extended simple point charge (SPC/E) model was picked for water molecules due to its simplicity and efficient computational cost [41]. Besides, it can also be depicted as an active rigid pair potential, including Lennard-Jones (LJ) and Columbic terms [42]. The three atoms of a water molecules have three interaction spots while they are allocated a point charge to induce long-range Columbic interactions. Moreover, oxygen atoms also show a Lennard Jones (LJ) potential to model the van der Waals (VDW) forces. As per the SPC/E model, oxygen and hydrogen atoms are allotted partial charges of q_O = 0. -8476e and qH = 0.4328e. Meanwhile, the H-O-H angle of 109.47^0 and O-H bond length of 0.1 nm was kept constant using the SHAKE algorithm [43]. A truncated Lennard Jones (LJ) (12-6) potential was used to measure the interatomic interaction of oxygen atoms of water molecules, salt ions, and carbon atoms in the graphene membrane as follows:

$$V_{ij} = 4\varepsilon\left(\left(\frac{\sigma}{r_{ij}}\right)^{12} - \left(\frac{\sigma}{r_{ij}}\right)^{6} - \left(\frac{\sigma}{r_c}\right)^{12} - \left(\frac{\sigma}{r_c}\right)^{6}\right). \quad (1)$$

Here, ε is the potential well depth, σ is the finite molecular distance at which point the interatomic potential is zero, r_{ij} is the intermolecular distance and lastly r_c is the cutoff distance. The intermolecular forces are curtailed at a distance of

Table 1. Details of the interaction parameters used in this work.

Interaction	$\varepsilon(ev)$	$\sigma(\dot{A})$
C-Cl	0.003619748	3.9240
C-Na	0.001350014	2.9876
C-O	0.00403278	3.283
C-H	0.0	0.0
Na-Cl	0.001702700	3.5116
Cl-O	0.005575083	3.8068
Cl-H	0.0	0.0
Na-O	0.002079272	2.8704
Na-H	0.0	0.0
Cl-Cl	0.004613823	4.4480
Na-Na	0.000641772	2.5752
H-H	0.0	0.0
O-O	0.006739	3.166
O-H	0	0.0

r_c = 1.0 nm in this work. The AIREBO potential was applied to model the planar interatomic interactions between carbon atoms in the graphene membrane [44]. Although the interaction parameters of Na^+ and Cl^- in the aqueous solutions were based on quantum calculations, oxygen atom interaction parameters were taken from the SPC/E model [45]. On the other hand, the interaction parameters between carbon and oxygen atoms were estimated from the Lorentz-Brethelot (L-B) mixing rule [46]. For any atomic molecules with charge, columbic interactions were also employed. Correspondingly, the dissolved salt ions Na^+ and Cl^- are assigned charges of q_{Na}= 1.0e and q_{Cl} = -1.0e. The interaction parameters used in this study is presented in Table 1 [12]. The particle-particle particle-mesh (PPPM) method was utilized to ensure precise long-range electrostatic interactions between all charged atomic types [46].

Newton's equations of motion were coordinated in the VERLET calculation with a simulation time step of 1.0 fs. Choosing a proper time step is a crucial issue for MD simulation since a large time step could led unstable MD simulation [47]. We have chosen the time step according to the literature with different type of fluid flow study and that also works in our system confirming with the dynamics [47-50]. All simulations were performed using LAMMPS [48]. The Maxwell-Boltzmann velocity distribution at 300 K was applied for assigning initial conditions of fluids. NVT (constant number of molecules, volume, and temperature) ensembles were initially used with a Nose-Hoover thermostat to preserve the system at 300 K in the equilibrium MD simulations. Individually, the feed and permeate sides have 1584 water molecules to meet the water density at 1 g/cm^3. Meanwhile, the feed side has 20 Na^+ and 20 Cl^- ions which result in a salt concentration in the feed region of 0.6 M.

For the first NVT ensemble, no pore was created and was equilibrated for 20 ns. After that, a pore 0.99 nm in diameter was created and equilibrated for an additional 3 ns. For all four cases, these two steps have been followed before continuing

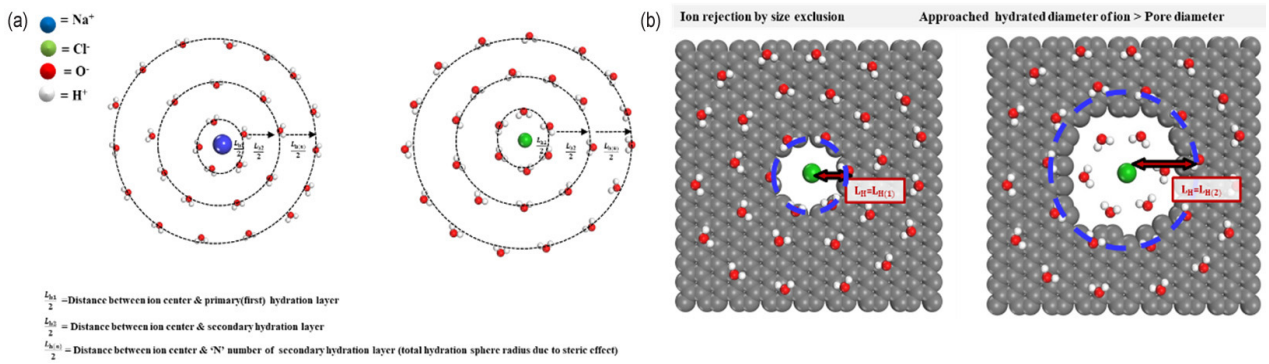

Fig. 2. (a) Typical illustration of the hydration layer of ion due to steric attraction for Na^+ and Cl^- ion; (b) approaching hydration boundary concept with different pore diameter.

to NEMD simulations. After the EMD, NEMD simulations were conducted to maintain flow for four different pore sizes of 0.568 nm, 0.994 nm, 1.420 nm and 1.9884 nm by moving the two specular reflection boundaries with the same velocity (1.5 ms^{-1}) in the z-direction through the fixed graphene membrane. The preferred velocity was 1.5 ms^{-1} because it well coordinated the molecular level with the continuum level properties for fluid in previous studies [40]. Using a higher specular reflection, the wall velocity may considerably disrupt the fluid thermodynamic properties, while applying a low velocity can increase the total computational time unreasonably.

2.2 Theoretical background

The structural configuration of water molecules induces polarity. As a result of their polarity and the strong local electric field around the ion, water molecules arrange themselves around the ions to form hydration layers [23]. In saltwater, positively charged Na^+ attracts the negatively charged oxygen atoms, while Cl^- attracts the positively charged hydrogen atoms of water molecules. The size of the ionic diameter is increased due to this hydration sphere (sum of the entire hydration layer) which is known as the steric effect of ions in an aqueous solution.

Fig. 2(a) illustrates the hydration sphere in saltwater for Na^+ and Cl^-. The first hydration layer of ions due to the strong attraction is known as the primary hydration layer. The second layer, up to an 'N' number of hydration layers, is known as the secondary hydration layer [31]. Here, the distance from the ion center to the primary hydration boundary is defined as, $\frac{L_{h_1}}{2}$, whereas L_{h_1} is the diameter for the first hydration layer. Similarly, L_{h_2} is the diameter of the secondary hydration layer. In this way, for an 'N' number of secondary hydration layers, the boundary is denoted as $\frac{L_{h_n}}{2}$ from the ion center. In Fig. 2(b), we marked the nearest hydration layer outside the pore diameter as the approached hydration diameter of ion transport ($\frac{L_{h_n}}{2}$). To reject the ion by the size-exclusion mechanism, the approached hydrated diameter needs to be larger than the pore diameter. Hence, when the pore diameter increased, the hydration diameters that approach the pore edges of the membrane need to be uplifted to reject the ion transportation.

3. Results and discussion

3.1 Density distributions of water and ions in the district of the porous membrane

As shown in Fig. 3(a), equilibrium molecular dynamics were used to determine the density distribution of water when the pore plug is off. The local density of water and salt ion concentrations were averaged for 20 ns by dividing the computational domain into slab bins with a length of 0.115 nm along the z-direction. Bin thickness was chosen to be ten times smaller than the molecular diameter of water to get a better visualization of the separation distance from the solid to the liquid region. The liquid transport and the liquid's properties are greatly influenced by both the molecular structure and intermolecular force of the liquid [40]. Clearly, the bulk density of water on both sides of the membrane is almost 1 g/cm^3 in Fig. 3(a) as anticipated. The density peak for water near the NPG membrane is observed due to the well-known density layering [51]. Due to the surface force and liquid-liquid strength in the nanoscale domain, liquid atoms adjacent to the solid surface drive in freezing mode and generate a solid-like liquid layer at a dissimilar molecular interface [52]. Though the layered liquid structure near the solid surface is not reflected at the continuum level, this can significantly influence the flow phenomena at the nanoscale due to the increase in interfacial density, viscosity, and pressure [53-55].

The density distribution of water molecules inside the nanopore is shown in Fig. 3(b) for a pore diameter of 1.98 nm. Fig. 3(b) shows, the atomic boundary position L' of pore diameter where the water molecule density drops 2 % from its bulk density [22]. From the density distribution inside the nanopore, L' was 0.3124 nm, 0.7426 nm, 1.20 nm, 1.83 nm for pore diameters of 0.568 nm, 0.99 nm, 1.42 nm, and 1.92 nm, respectively. After that, (L - 2 σ_{c-c}) is defined as the atomic boundary position L'' of the pore diameter whereas σ_{c-c} is atomic radius of the carbon atom.

3.2 Pressure distribution of saltwater across the system

Pressure is developed in the feed and permeate region by the movement of the SRW at a constant speed (1.5 ms^{-1}). The pressure distribution for only one pore diameter (L) of 0.994 nm is shown in Fig. 3(c) for a system of LJ+Columbic interaction between ion and water.

The average of the three symmetrical ordinary stress segments in the Cartesian coordinate system from the IK expression is used to determine pressure [56-58]. The bin size for the pressure distribution was also chosen to be 0.115 nm to better describe the molecular interactions in compliance with the density distribution. Fig. 3(c) shows the pressure distribution in the z-direction, which displays ambivalence close to the interface. Due to the higher surface force of the solid-water interface compared with the water-water forces, the local shear stress near the interface is increased, which eventually generates a pressure peak close to the interface on both sides of the system [39, 56]. A similar thing was seen in the earlier studies where it was established that getting an anisotropic type of pressure close to the interface is very fundamental to different type of solid-liquid study [12, 39]. In MD simulation, it is vital to validate the thermodynamic properties of the system with the existing literature. Our pressure and density distribution ensured that our system is validated according to the literature. To find the pressure difference, the constant bulk pressure on the feed p_f and permeate p_p sides are given as follows:

$$\Delta P = P_f - P_p . \tag{2}$$

From Fig. 3(d), it is observed that the pressure difference along the z-direction is reduced in a non-linear way when the pore diameter is increased, although the specular reflective wall velocity is the same for all cases. However, for the LJ+ Columbic interaction between water and ion, the pressure difference is less than in the cases of LJ interactions between water and ions. As pore diameter increases, the saltwater flow area is increased. As a result, the shear stress between the molecules of saltwater decreases on the feed side. Due to the decreasing shear stress in the feed side, the pressure drop of the system is reduced with increasing the pore diameter. Although these pressure drop values are really high for a practical field desalination application, computationally it is very general to use a high pressure drop value if the research objective is not limited to only get a higher salt rejection and water flux [12, 20]. Additionally, it would be computationally very expensive to generate a water flow in our smallest nanopore (0.568 nm) using a low SRW velocity which can generate a low pressure difference for all of the pore cases.

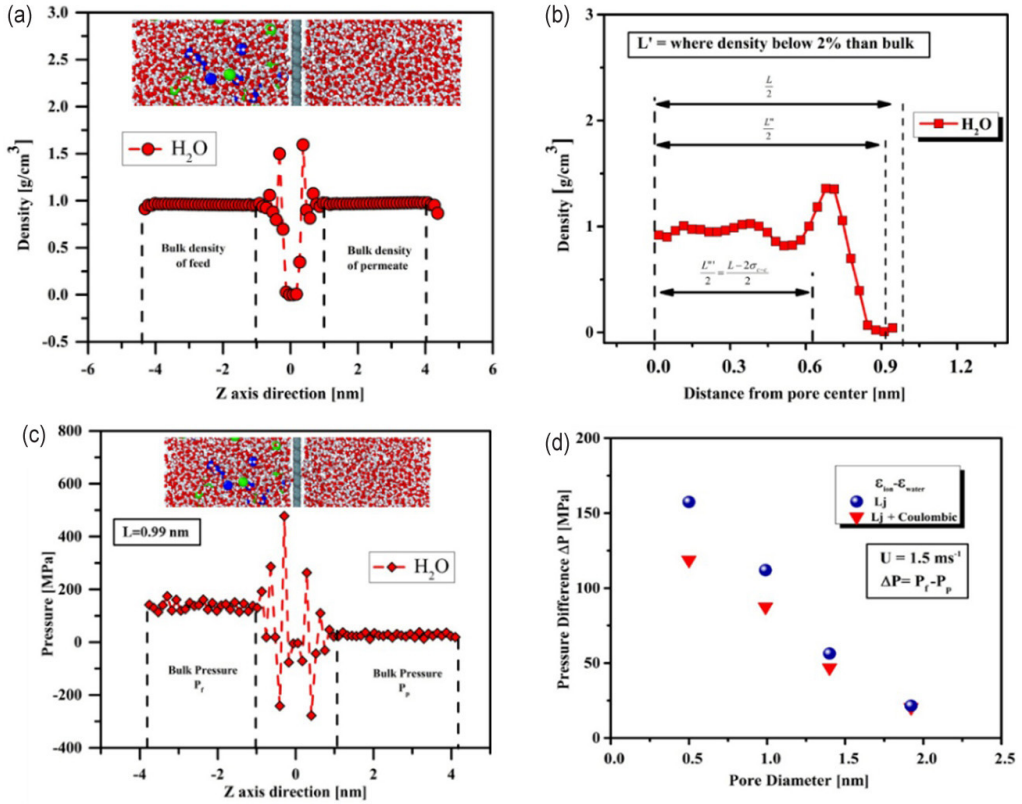

Fig. 3. (a) Mass density distribution of water; (b) determining pore boundary L' using water's radial density peak; (c) pressure distribution along the z-axis direction while two specular reflection boundaries are moving at 1.5 ms^{-1}; (d) pressure difference varied for various pore sizes for LJ and LJ+ Columbic interaction between ion and water molecules.

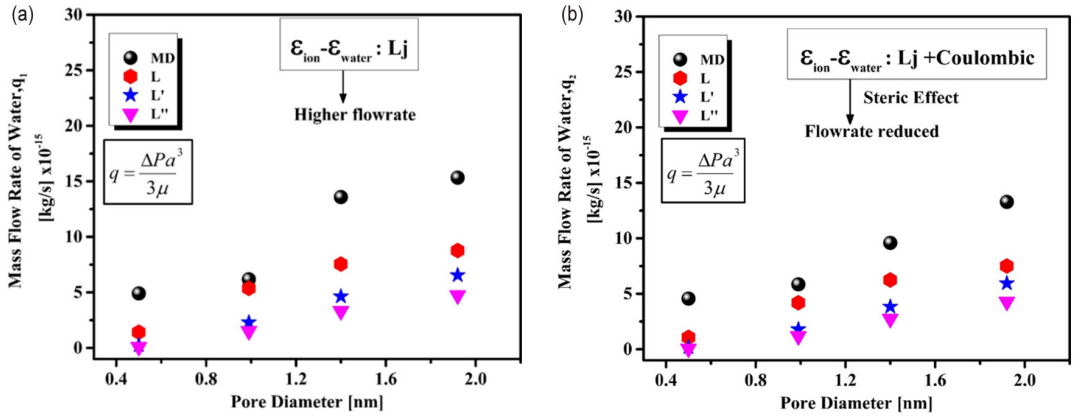

Fig. 4. (a) Water mass flow rate relation with pore diameter with atomic boundary position for LJ interaction between ion and water; (b) water mass flow rate relation with pore diameter with atomic boundary position for LJ+ Coulomb interaction between ion and water.

3.3 Comparison of water mass flow rate

The water cluster around the ion (or steric effect) is caused by the Columbic interactions between the ion and water molecules [7]. To visualize the steric effect on water flow rate, the water mass flow rate is depicted separately both for LJ interactions and LJ+ Columbic interactions between the water and ion along with atomic boundary position of the pore diameter in Figs. 4(a) and (b). In both cases, all the molecular interaction and other parameters are the same except the ion-water interactions. The MD flow rate was calculated from the water molecule's change of time rate along the feed reservoir and multiplied by the number of water molecules that filled the volume. Each water molecule fills a volume of 0.03231 nm^3 in each reservoir. Interestingly, the water mass flow rate is reduced when the steric effect is present (LJ+Columbic interactions between water and ions). A possible explanation for this phenomenon is related to water cluster formation around the ions due to the electrostatic interactions. In the presence of a steric effect, the ions hinder the water molecules from moving freely, which ultimately reduces the water flow rate.

In addition to that, for three different boundary positions (i.e., pore diameters), the Sampson flow prediction was calculated from the Sampson flow equation that was solved from the Stokes equations for pressure-driven flow through an infinitely thin circular orifice [59]. The mass flow rate from the Sampson flow rate equation could be obtained from the equation below:

$$q = \frac{\Delta P a^3}{3\mu}. \tag{3}$$

Here, q denotes the volumetric flow rate, a denotes the pore radius and μ denotes the viscosity of the fluid. The viscosity of saltwater is 850-860 μPa, which is used in the Sampson flow rate calculation [60]. To predict the Sampson flow rate, the water flow rate was also reduced for the steric affected case, like the MD predicted result. It is apparent that the predicted Sampson flow rate also needs to be reduced as the pressure difference decreased for each pore diameter of the steric affected case, due to the linear relationship between pressure and mass flow rate. In both steric and non-steric affected cases, the Sampson flow rate prediction is lower than the MD predicted magnitude. Since the Sampson flow overpredicts the hydrodynamic resistance of the graphene Nanopore, the water mass flow rate decreases for the Sampson flow prediction based on MD [61]. Moreover, when the atomic boundary position of L' and L'' are applied to the Sampson flow rate prediction, it starts to deviate more from the MD predicted result. This indicates that applying the atomic boundary position of nanopores in the Sampson flow model does not hold the same prediction for water mass flow rate as it holds for simple fluid flow [62]. The long-range Columbic interactions of the water molecules themselves could play a key role here in this variance.

3.4 Comparison of water velocity profile

To investigate the cause of the mass flow rate reduction of the water molecule in the presence of a steric effect, we analyzed the velocity distribution of water molecules at the pore and also for the overall system. To maintain the brevity, only the velocity distribution of 1.42 nm pore diameter is shown in Figs. 5(a)-(c). Fig. 5(a) illustrates the comparison between the velocity of water molecules for the entire system for LJ and LJ+ Columbic interaction between water and ions. When the ions-water have Columbic interaction, the ions attract the water molecules, strongly hindering their usual movement. As a result, the water velocity becomes lower for the steric affected case, and this difference between these two cases is more apparent at the center of the pore. In Figs. 5(b) and (c), the velocity profile at the pore center is shown from the MD simulation along with the Sampson flow equation with a different boundary position of pore diameter. Applying Sampson's stream function solution in cylindrical coordinates, the velocity profile for r position inside the pore can be expressed as follows:

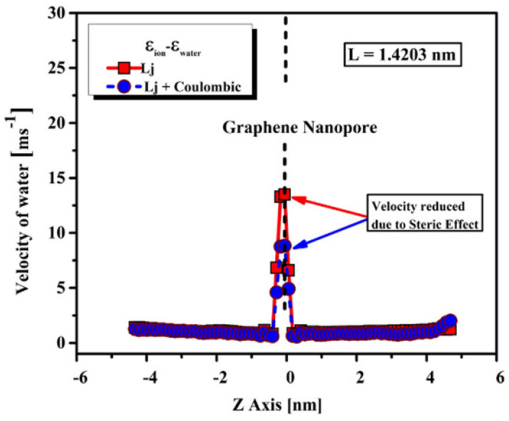

(a)

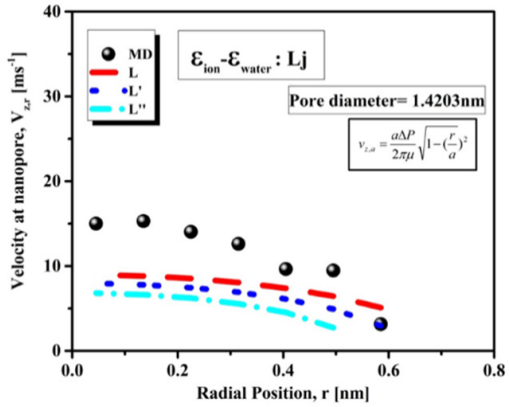

(b)

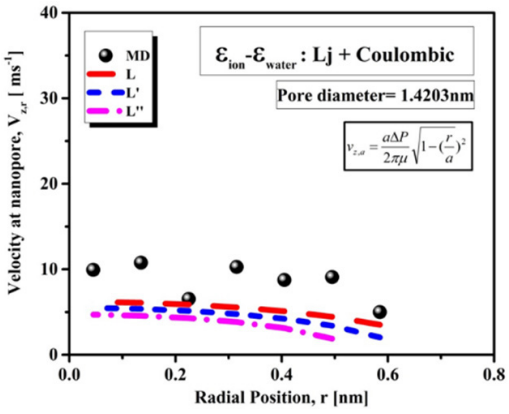

(c)

Fig. 5. (a) Water velocity distribution for pore diameter of 1.42 nm; (b) water velocity inside the nanopore for LJ interactions between ions and water for a pore diameter of 1.42 nm; (c) water velocity inside the nanopore for LJ+ Columbic interactions between ions and water for a pore diameter of 1.42 nm.

$$V_{z,r} = \frac{a\Delta P}{2\pi\mu}\left(\sqrt{(1-\left(\frac{r}{a}\right)^2}\right). \quad (4)$$

Fig. 5(c) shows that, a cylindrical bin is used to calculate the velocity profile of water from MD, with a radius equal to the pore radius and length equal to the diameter of a single carbon atom. The cylindrical bin axis is set along the Z direction of the pore center, and the bin is also divided into multiple concentric circle bins to gather the velocity data in the radial direction of the pore. The multiple concentric circle bins are divided to get the maximum water molecules in each bin. The data are averaged for 0.4 ns when the water flow is established across the nanopore for a 1.42 nm diameter nanopore. The velocity profile is also reduced for different boundary conditions with the Sampson flow model for the steric-affected system case, and it also deviates from the MD value, maintaining consistency with the flow rate results.

3.5 Defining the primary hydration boundary of ions

The ionic concentration distribution is represented in Fig. 6(a) along the z-direction while ensuring that no ion passed through the nanopore in EMD without applying pressure. The bulk ionic concentrations for Na^+ and Cl^- are almost equal and matched with the theoretically calculated value of 0.6 M. Although our focus is to investigate any impact to ions transportations due to a shift of the atomic boundary position of pore diameter, equal concentrated sodium and chlorine ion is presented in this system due to maintaining the charge neutrality for added charge in the system. The primary hydration layer boundary [L_{h1}] is measured precisely, using the radial distribution function (RDF). Fig. 6 shows that, the radius of the primary shell boundary [$\frac{L_{h1}}{2}$] is determined using the RDF. The first density peak in the radial distribution function indicates the starting region of the primary hydration layer, while the first minimum after the first density peak is considered to be the radius of the primary hydration layer from the ion center. For Na^+, the peak in the RDF indicates the strong electrostatic interactions with O^- atoms of the primary hydration layer. For Cl^-, it defines the strong electrostatic interactions with H^+ atoms of its primary hydration layer. The first minimum density drop indicates the strong repulsion between the atoms of the same charge.

The primary hydration layer radii of Na^+ and Cl^- in this study are as 0.37 nm and 0.39 nm, respectively, which matched closely with the previous studies [26, 63]. After the first hydration layer, the second and the third hydration layers are found to be 0.62 nm and 0.85 nm from the chlorine ion center, respectively. For sodium, the second and the third hydration layer were found at 0.62 nm and 0.84 nm from the ion center, respectively. According to the literature, the subsequent layer after the innermost layer is spaced at 0.2-0.23 nm [24].

3.6 Relating atomic boundary positon of pore diameter with ion transportation

When the pore diameter is smaller than the hydration shell of the ion, the hydration shell would not fit inside the pore. However, to fit inside a smaller diameter pore, some water mole-

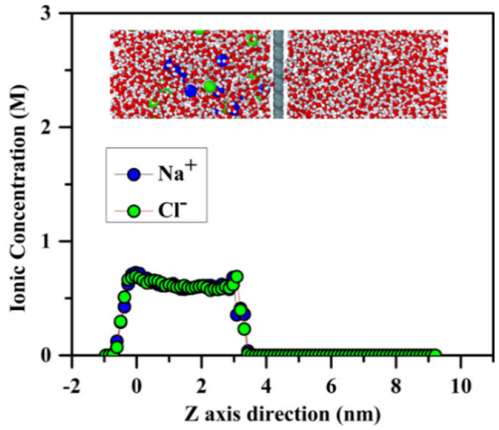

(a)

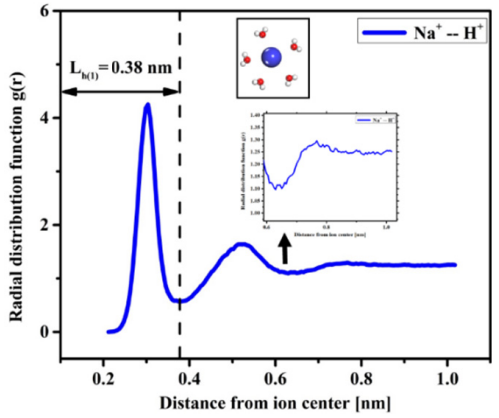

(b)

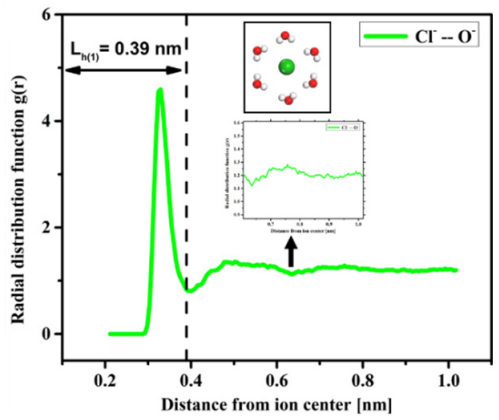

(c)

Fig. 6. (a) Density distribution of ions; (b) defining hydration radius of sodium ions with the radial distribution function of water molecules around sodium ions; (c) defining hydration radius of chlorine ions with the radial distribution function of water molecules around chlorine ions.

cules can be removed from the hydration shell at an energy cost [7, 24]. This phenomenon can change the initial total hydration diameter of the ion. The approached hydration boundary is denoted as the closest hydration layer to the pore edge that needs to be dehydrated so that the ion can be transported through the pore. Therefore, the change of the approached hydration diameter will depend on the pore diameter. For example, to fit and transport through a diameter of 0.56 nm, chlorine's first hydration layer (0.76 nm) requires dehydration. However, while transporting through the pore diameter of 0.99 nm, chlorine's second hydration layer needs to be dehydrated, although the first hydration layer can be present during transportation. In that case, the approached hydration diameter is changed to the length of the second hydration shell (1.24 nm). This tendency of changing the approached hydration boundary with the pore diameter has been depicted in Fig. 7(a) and is due to the dehydration in ion transportation.

Based on our objective monitoring atomic boundary position of pore diameter effect on ion transportation and for conciseness, we have shown our analysis only for the chlorine since the considerations are the same for others ion too [24]. We observed that the approached hydration boundary appeared to be broad with the pore diameter increment. However, in that case, the attraction between the ion and the water molecules on that specific layer is decreased according to the Coulombs law. Therefore, the energy cost to remove the water molecules from the more extended hydration layer should be less compared to the hydration layer nearest to the ion. To express this, we used the model proposed by Zwolak et al. where the energy barrier to dehydrate the water molecules from the hydrated layer was presented as a function of pore radius [24]. That model is assumed to be valid for an ion concentration less than 1M and with the absence of surface charge within the pore, which are also mutual in our system. In the model, the internal energy is contained in a partially intact hydration layer as $U_i = f_i U_i^o$; Here f_i denotes the fraction of the hydration layer present inside the pore area. Here, f_i represents the hydration layer radius R_i and a specific pore radius a by:

$$f_i = 1 - \sqrt{\left(1 - \frac{a}{R_i}\right)^2}. \tag{5}$$

U_i^o is the energy difference between the hydration layer and water in the bulk. Here,

$$U_i^o = \left(\frac{e^2}{8\pi \in_o}\right)\left(1 - \frac{1}{k}\right)\left(\frac{1}{R_i^0} - \frac{1}{R_i^I}\right). \tag{6}$$

Here, K represents the dielectric constant of water and R_i^0 denotes the hydrated layers present for the outer and inner pore area. The internal energy barrier as a function of pore radius is denoted by

$$\Delta U\left(R_p\right) = \sum_i f_i (a-1) U_i^0. \tag{7}$$

From this model and Fig. 7(b), it is evident that our initial thought about the decrease of the energy cost for dehydration with the pore boundary increase is valid. However, to see the impact of different atomic boundary positions on ion transporta-

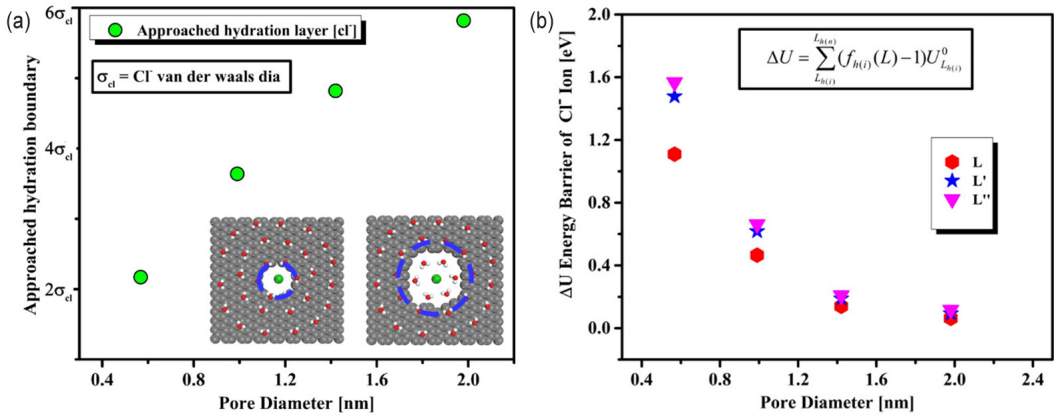

Fig. 7. (a) Approached hydrated boundary relation to the pore diameter; (b) energy barrier for chlorine ion with pore diameter by applying the atomic boundary position.

tion, we have applied the atomic boundary position of pore diameter L, L' and L'' here. Interestingly, when the pore diameter is below 1 nm, the energy barrier of the ion for a pore diameter deviates significantly for the different atomic boundary positions of pore diameter. However, a vice versa situation happens for larger pore diameters. In fact, the energy barriers almost matches for L, L' and L'' when the pore diameter is 1.988 nm. Due to the scale effect, the energy barrier difference becomes more apparent for different atomic boundary positions of pore diameter when the pore diameter becomes less than 2 nm [59, 64].

To see the impact of the deviation of the energy barrier of an ion on ion transportation, the input is the calculated energy for the chlorine ion in the feed side from the MD simulation. The input energy E_i values were found at 68.67 eV, 8.5 eV, 2.50 eV, and 2.37 eV for the pore diameter of 0.568 nm, 0.99 nm, 1.42 nm, and 1.94 nm, respectively, considering the kinetic and virial stress of chlorine along the flow axis. The input energy of chlorine ion is averaged for each pore diameter until at least 160 water molecules are transported. To predict the chlorine ion transportation theoretically for different atomic boundary positions of pore diameter, the ion transportation prediction is proposed as to the ratio of the total chlorine ions input energy and the total energy barrier of chlorine ion as a function of pore radius. Therefore, the ion rejection I for different atomic boundaries becomes:

$$I = 1 - \left(\frac{E_i}{\Delta U} \right). \tag{8}$$

However, to maintain a consistent comparison for our theoretical and MD prediction, the chlorine ion rejection from MD was also calculated for the time when more than 160 water molecules transported through the nanoporous graphene membrane for all the pore diameter cases. This reference time is selected to get a reasonable computational time and have a proper view of the ion rejection from a small to a big pore diameter. Fig. 8 shows that the ion rejection prediction could be

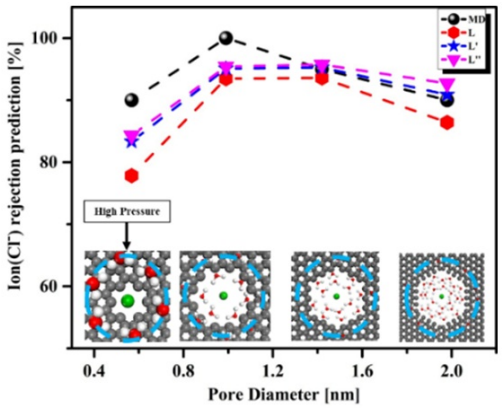

Fig. 8. Chlorine ion rejection prediction for different atomic boundary positions of pore diameter and from MD simulation.

shifted for the different atomic pore boundary positions. Due to the atomic boundary position moving towards the pore center, the resistance to the ion transportation incline ultimately affected the ion rejection. The difference between the MD predicted ion rejection and our theoretically predicted ion rejection is more visible when the pore diameters become less than 1 nm. A possible explanation is linked to the van der Waals and Columbic interactions between the ion and the membrane. When the pore is very narrow with boundary conditions, the ion faces exponentially increased high repulsion from the graphene membrane.

Thus, either the ion needs to move away to the feed side or the permeate side, depending on the input energy. If the input energy is high enough, the ion is pushed through the nanopore and goes to the permeate side. In this consequence, it is observed that for a pore diameter of 0.568 nm, all the hydration shells need to be dehydrated to transport through this pore. It was noticed that for the 0.568 nm pore, the input energy is 8 times higher than the closest pore diameter (0.99 nm) case. Therefore, if at least one chlorine ion was transported through this pore diameter, it is detached from the entire hydration layer with this input energy. A similar phenomenon could be started

with all the chlorine ions of the system, and they started to transport more rapidly only with their bare ionic diameter (0.34 nm) or with a partial hydration shell [65]. Due to transport with a much lower diameter than the size, including the first hydration shell, the ion rejection for the 0.568 nm pore goes against the inversely proportional trends with ion rejection and pore diameter. Besides this, one different phenomenon could be happened in ionic fluid flow through the nanopore depending on the nanopore diameter size. If the nanopore diameter is very small, the energy barrier is very high which accumulates the ions to plug the pore that can increase the pressure drop along with decreasing the flowrate. However, if the nanopore diameter is enough increased as like our 1.98 nm diameter where the ion transportation barrier is nearly zero, then this ion plugging issue in the nanopore could be negligible. In our work, we didn't consider this issue since we have a various size of pore diameter and our objective was not to establish an economical model for water desalination which have already done in the past literatures [12, 20]. However, to make an efficient desalination model with a specific pore size it is recommended to consider this ion plugging issue to get an effective model.

The most noticeable point from Fig. 8 is that the MD prediction ion rejection value is most closely matched with the atomic boundary position of L' for the pore diameter cases 1.42 nm and 1.98 nm. The center to center atomic boundary position L predicts low resistance for ion transportation, whereas L'' over-predicts the higher resistance for ion transportation. Therefore, for these two atomic boundary positions, the ion rejection could be less approximate than the atomic boundary position of L'. The effective pore diameter for ion rejection is that which forces the hydration layer to be partially broken off [24]. According to this thought and the observed result from the pore diameter of 1.42 nm and 1.98 nm, L' could be the approximate atomic boundary position for ion rejection since it also corresponds to the dense core area of water molecules inside the nanopore. However, the atomic boundary position becomes more difficult to approximate for ion rejection, when the pore diameter becomes less than 1 nm. The van der Waals repulsion is too high in this case to precisely approximate the boundary position of pore diameter as a basis for comparison of theoretical and MD predicted results.

However, the similarity and deviation of the theoretical and MD predicted ion rejection indicates the atomic boundary position effect, which was previously addressed for a simple fluid flow [59]. As to the water flow rate deviation from the MD predicted result, the ion rejection can also be significantly changed due to the pore diameter's atomic boundary position effect when the scale becomes less than 2 nm. In synopsis, since the Van der Waals force and the Columbic interaction of the molecules becomes significantly apparent at the molecular level, a small change in the atomic boundary position could lead to a greater change in the resistance of water and ion transportation. That shift in the resistance of nanopore diameter due to the atomic boundary position could significantly impact the flow phenomenon of ions along with water transportation.

4. Conclusion

This study emphasized the impact of the pore diameter's atomic boundary position on ion transportation using pressure-driven flow through a nanoporous graphene membrane. The effect of the atomic boundary position of the pore diameter is related to the ion's hydrations layers. Moreover, the hydration layer is the outcome of the steric effect of ions, which also modifies the water velocity and flow rate. The impact of the steric effect on water flow properties has been visualized by alternating the LJ and LJ+ Columbic force interactions between the water and ions. Apart from that, the velocity and flow rate from the Sampson flow model are lower than the MD predicted result for both steric and non-steric-affected cases. A hypothesis of the approached hydration boundary connection with the pore diameter has been defined for water and ion transportation. Employing this assumption, the energy barrier of the ion transport as a function of the pore diameter was illustrated for each of the atomic boundary positions of pore diameter. Consequently, the theoretical ion transportation is proposed with the ratio of input energy of the total ion and total energy barrier of the ion transport as a function of the pore diameter.

The theoretical ion rejection is compared with the MD predicted ion rejection to observe the importance of the pore diameter's atomic boundary position on ion transportation. It is noticed that the theoretical ion rejection significantly deviated for the different atomic boundary positions of pore diameter when the pore diameter was less than 1 nm. However, at diameters greater than 1 nm, the theoretical ion rejection is identical to the MD predicted result for the atomic boundary position stated to the 2 % water density drop inside the nanopore. Moreover, it is also observed that if the entire hydration layer is broken, the ion rejection is significantly reduced going against the inversely proportional relationship with pore diameter. In future work, we would like to explore the theoretical ion rejection prediction with lower input energy which was not assessed in this work due to the computational time frame. Discussing proper atomic boundary position for ion transportation and separation through our investigations will have implications for t desalination experiments and the reverse osmosis plants for water purification.

Acknowledgements

This work was supported by the National Research Foundation of Korea (NRF) grant funded by the Korean government (MSIT) (NRF-2019R1A2C1004661).

Nomenclature

f_i : Fraction of the hydration layer inside the pore area
ΔU : Energy barrier for single ion transport
E_i : Input energy for chlorine
L : Pore diameter
a : Pore radius

L_h : Hydration diameter of ion
R_i : Hydration layer radius
V : Interaction potential function
$V_{z,r}$: Velocity inside pore
q : Volumetric flow rate of fluid
σ : Diameter of molecules (zero potential distance)
μ : Viscosity of fluid

References

[1] P.H.W. Gleick, *Water in Crisis*, Oxford University Press (1993).
[2] WWAP and UNESCO, *The United Nations World Water Development Report 2019: Leaving No One Behind*, United Nations Educational, Scientific and Cultural Organization (2019).
[3] E. Jones, The state of desalination and brine production: A global outlook, *Sci. Total Environ.*, 657 (2019) 1343-1356.
[4] M. A. Shannon, P. W. Bohn, M. Elimelech, J. G. Georgiadis, B. J. Marinas and A. M. Mayes, Science and technology for water purification in the coming decades, *Nanoscience and Technol.* (2009) 337-346.
[5] S. Zhao, Recent developments in forward osmosis: Opportunities and challenges, *J. Memb. Sci.*, 396 (2012) 1-21.
[6] M. Qasim, Reverse osmosis desalination: a state-of-the-art review, *Desalination*, 459 (2019) 59-104.
[7] B. Corry, Mechanisms of selective ion transport and salt rejection in carbon nanostructures, *MRS Bull.*, 42 (4) (2017) 306-310.
[8] F. Fornasiero, Ion exclusion by sub-2-nm carbon nanotube pores, *Proc. Natl. Acad. Sci.*, 105 (45) (2008) 17250-17255.
[9] Y. Wang et al., Nanopore sequencing technology, bioinformatics and applications, *Nat. Biotechnol.*, 39 (11) (2021) 1348-1365.
[10] M. Heiranian, A. B. Farimani and N. R. Aluru, Water desalination with a single-layer MoS_2 nanopore, *Nat. Commun.*, 6 (1) (2015) 8616.
[11] P. R. Kidambi et al., Assessment and control of the impermeability of graphene for atomically thin membranes and barriers, *Nanoscale*, 9 (24) (2017) 8496-8507.
[12] C. T. Nguyen and A. Beskok, Saltwater transport through pristine and positively charged graphene membranes, *J. Chem. Phys.*, 149 (2) (2018) 024704.
[13] A. K. Geim and K. S. Novoselov, The rise of graphene, *Nanoscience and Technology*, UK (2009) 11-19.
[14] K. Cao et al., Elastic straining of free-standing monolayer graphene, *Nat. Commun.*, 11 (1) (2020) 284.
[15] D. He, Engineered graphene materials: synthesis and applications for polymer electrolyte membrane fuel cells, *Adv. Mater*, 29 (20) (2017) 1601741.
[16] M. Liu, R. Zhang and W. Chen, Graphene-supported nanoelectrocatalysts for fuel cells: synthesis, properties, and applications, *Chem. Rev.*, 114 (10) (2014) 5117-5160.
[17] D. Cohen-Tanugi and J. C. Grossman, Mechanical strength of nanoporous graphene as a desalination membrane, *Nano Lett.*, 14 (11) (2014) 6171-6178.
[18] A. Nicolaï, B. G. Sumpter and V. Meunier, Tunable water desalination across graphene oxide framework membranes, *Phys. Chem. Chem. Phys.*, 16 (18) (2014) 8646.
[19] J. Goldsmith and C. C. Martens, Pressure-induced water flow through model nanopores, *Phys. Chem. Chem. Phys.*, 11 (3) (2009) 528-533.
[20] D. Cohen-Tanugi and J. C. Grossman, Water desalination across nanoporous graphene, *Nano Lett.*, 12 (7) (2012) 3602-3608.
[21] D. Konatham, Simulation insights for graphene-based water desalination membranes, *Langmuir*, 29 (38) (2013) 11884-11897.
[22] M. E. Suk and N. R. Aluru, Molecular and continuum hydrodynamics in graphene nanopores, *RSC Adv.*, 3 (24) (2013) 9365.
[23] M. Zwolak, J. Wilson and M. Di Ventra, Dehydration and ionic conductance quantization in nanopores, *J. Phys. Condens. Matter*, 22 (45) (2010) 454126.
[24] M. Zwolak, J. Lagerqvist and M. Di Ventra, Quantized ionic conductance in nanopores, *Phys. Rev. Lett.*, 103 (12) (2009) 128102.
[25] F. Risplendi, Fundamental insights on hydration environment of boric acid and its role in separation from saline water, *J. Phys. Chem. C*, 124 (2) (2020) 1438-1445.
[26] M. E. Suk and N. R. Aluru, Ion transport in sub-5-nm graphene nanopores, *J. Chem. Phys.*, 140 (8) (2014) 084707.
[27] J. P. K. Abal, J. R. Bordin and M. C. Barbosa, Salt parameterization can drastically affect the results from classical atomistic simulations of water desalination by MoS_2 nanopores, *Phys. Chem. Chem. Phys.*, 22 (19) (2020) 11053-11061.
[28] O. Beckstein and M. S. P. Sansom, The influence of geometry, surface character, and flexibility on the permeation of ions and water through biological pores, *Phys. Biol.*, 1 (1) (2004) 42-52.
[29] J. R. Bordin, Ion fluxes through nanopores and transmembrane channels, *Phys. Rev. E*, 85 (3) (2012) 031914.
[30] B. Pinter, On the origin of the steric effect, *Phys. Chem. Chem. Phys.*, 14 (28) (2012) 9846.
[31] B. Tansel, Significance of hydrated radius and hydration shells on ionic permeability during nanofiltration in dead end and cross flow modes, *Sep. Purif. Technol.*, 51 (1) (2006) 40-47.
[32] L. A. Richards, The importance of dehydration in determining ion transport in narrow pores, *Small*, 8 (11) (2012) 1701-1709.
[33] A. Tongraar and B. Michael Rode, Dynamical properties of water molecules in the hydration shells of Na+ and K+: ab initio QM/MM molecular dynamics simulations, *Chem. Phys. Lett.*, 385 (5-6) (2004) 378-383.
[34] K. Coutinho, Electronic polarization of liquid water: converged Monte Carlo-quantum mechanics results for the multipole moments, *Chem. Phys. Lett.*, 369 (3-4) (2003) 345-353.
[35] S. W. Rick and B. J. Berne, The aqueous solvation of water: a comparison of continuum methods with molecular dynamics, *J. Am. Chem. Soc.*, 116 (1993) 3949-3954.
[36] J. Aqvist and T. Hansson, On the validity of electrostatic linear response in polar solvents, *J. Phys. Chem.*, 100 (22) (1996) 9512-9521.
[37] S. Sahu, M. Di Ventra and M. Zwolak, Dehydration as a universal mechanism for ion selectivity in graphene and other

atomically thin pores, *Nano Lett.*, 17 (8) (2017) 4719-4724.
[38] C. T. Nguyen, M. Barisik and B. Kim, Wetting of chemically heterogeneous striped surfaces: Molecular dynamics simulations, *AIP Adv.*, 8 (6) (2018).
[39] M. Barisik and A. Beskok, Equilibrium molecular dynamics studies on nanoscale-confined fluids, *Microfluid. Nanofluidics*, 11 (3) (2011) 269-282.
[40] M. R. Hasan and B. Kim, Molecular transportation phenomena of simple liquids through a nanoporous graphene membrane, *Phys. Rev. E*, 102 (3) (2020) 033110.
[41] Vishnu Prasad K., S. K. Kannam, R. Hartkamp and S. P. Sathian, Water desalination using rapheme nanopores: influence of the water models used in simulations, *Phys. Chem. Chem. Phys.*, 20 (23) (2018) 16005-16011.
[42] Grigera and T. P. Straatsma, The missing termi n effective pair potentials, *The Journal Phys. Chem.*, 91 (24) (1987) 6269-6271.
[43] J. P. Ryckaert, G. Ciccotti and H. J. C. Berendsen, Numerical integration of the cartesian equations of motion of a system with constraints: molecular dynamics of n-alkanes, *J. Comput. Phys.*, 23 (3) (1977) 327-341.
[44] S. J. Stuart, A. B. Tutein and J. A. Harrison, A reactive potential for hydrocarbons with intermolecular interactions, *J. Chem. Phys.*, 112 (14) (2000) 6472-6486.
[45] M. Patra and M. Karttunen, Systematic comparison of force fields for microscopic simulations of NaCl in aqueous solutions: Diffusion, free energy of hydration, and structural properties, *J. Comput. Chem.*, 25 (5) (2004) 678-689.
[46] D. J. Allen, P. Michael and Tildesley, *Computer Simulation of Liquids*, Oxford University Press (2007).
[47] S. Kim, Issues on the choice of a proper time step in molecular dynamics, *Phys. Procedia*, 53 (2014) 60-62.
[48] S. Plimpton, Fast parallel algorithms for short-range molecular dynamics, *J. Comput. Phys.*, 117 (1) (1995) 1-19.
[49] M. Masuduzzaman and B. Kim, Unraveling the molecular interface and boundary problems in an electrical double layer and electroosmotic flow, *Langmuir*, 38 (23) (2022) 7244-7255.
[50] C. T. Nguyen and A. Beskok, Water desalination performance of h-BN and optimized charged graphene membranes, *Microfluid. Nanofluidics*, 24 (5) (2020).
[51] C. T. Nguyen and B. Kim, Stress and surface tension analyses of water on graphene-coated copper surfaces, *Int. J. Precis. Eng. Manuf.*, 17 (4) (2016) 503-510.
[52] M. Masuduzzaman and B. Kim, Scale effects in nanoscale heat transfer for fourier's law in a dissimilar molecular interface, *ACS Omega*, 5 (41) (2020) 26527-26536.
[53] T. Q. Vo and B. Kim, Interface thermal resistance between liquid water and various metallic surfaces, *Int. J. Precis. Eng. Manuf.*, 16 (7) (2015) 1341-1346.
[54] B. H. Kim, A. Beskok and T. Cagin, Thermal interactions in nanoscale fluid flow: molecular dynamics simulations with solidliquid interfaces, *Microfluid. Nanofluidics*, 5 (4) (2008) 551-559.
[55] L. Xue, P. Keblinski, S. R. Phillpot, S. U.-S. Choi and J. A. Eastman, Effect of liquid layering at the liquid-solid interface on thermal transport, *Int. J. Heat Mass Transf.*, 47 (19-20) (2004) 4277-4284.
[56] M. Masuduzzaman and B. H. Kim, Effects of dissimilar molecular interface and ion-concentration on wetting characteristics of nanodroplets, *Microfluid. Nanofluidics*, 25 (6) (2021) 1-14.
[57] J. H. Irving and J. G. Kirkwood, The statistical mechanical theory of transport processes IV. The equations of hydrodynamics, *J. Chem. Phys.*, 18 (1950) 817.
[58] B. D. Todd, D. J. Evans and P. J. Daivis, Pressure tensor for inhomogeneous fluids, *Phys. Rev. E*, 52 (1995) 1627.
[59] R. A. Sampson, XII. On Stokes's current function, *Philos. Trans. R. Soc. London.*, 182 (1891) 449-518.
[60] C. T. Nguyen and A. Beskok, Saltwater transport through pristine and positively charged graphene membranes, *J. Chem. Phys.*, 149 (2) (2018).
[61] M. Heiranian, A. Taqieddin and N. R. Aluru, Revisiting sampson's theory for hydrodynamic transport in ultrathin nanopores, *Phys. Rev. Res.*, 2 (4) (2020) 43153.
[62] J. Al Hossain and B. H. Kim, Scale effect on simple liquid transport through a nanoporous graphene membrane, *Langmuir*, 37 (21) (2021) 6498-6509.
[63] I. S. Joung and T. E. Cheatham, Molecular dynamics simulations of the dynamic and energetic properties of alkali and halide ions using water-model-specific ion parameters, *J. Phys. Chem. B*, 113 (40) (2009) 13279-13290.
[64] L. Bocquet and E. Charlaix, Nanofluidics, from bulk to interfaces, *Chem. Soc. Rev.*, 39 (3) (2010) 1073-1095.
[65] A. Bondi, van der Waals volumes and radii, *J. Chem. Phys.*, 68 (3) (1964) 441-451.

Morshed Mahmud is a Master of science candidate in Mechanical Engineering, University of Ulsan, Korea. His research interests are Molecular Dynamics simulation, micro-/nano-fluidics, ion transportation, desalination.

BoHung Kim is an Associate Professor in School of Mechanical Engineering, University of Ulsan, Korea. He received his Ph.D. degree from Department of Mechanical Engineering, Texas A&M University, United States. His research interests are molecular neuroscience, Molecular Dynamics and nanoscale gas/liquid flow, and numerical methods.